

Coupling strength versus coupling impact in nonidentical bidirectionally coupled dynamics

Petroula Laiou

Department of Information and Communication Technologies, Universitat Pompeu Fabra, Barcelona, 08018 Spain

Ralph G. Andrzejak

*Department of Information and Communication Technologies, Universitat Pompeu Fabra, Barcelona, 08018 Spain
and Institut de Bioenginyeria de Catalunya (IBEC), Baldori Reixac 15-21, Barcelona 08028, Catalonia, Spain*

(Received 3 June 2016; revised manuscript received 6 November 2016; published 20 January 2017)

The understanding of interacting dynamics is important for the characterization of real-world networks. In general, real-world networks are heterogeneous in the sense that each node of the network is a dynamics with different properties. For coupled nonidentical dynamics symmetric interactions are not straightforwardly defined from the coupling strength values. Thus, a challenging issue is whether we can define a symmetric interaction in this asymmetric setting. To address this problem we introduce the notion of the coupling impact. The coupling impact considers not only the coupling strength but also the energy of the individual dynamics, which is conveyed via the coupling. To illustrate this concept, we follow a data-driven approach by analyzing signals from pairs of coupled model dynamics using two different connectivity measures. We find that the coupling impact, but not the coupling strength, correctly detects a symmetric interaction between pairs of coupled dynamics regardless of their degree of asymmetry. Therefore, this approach allows us to reveal the real impact that one dynamics has on the other and hence to define symmetric interactions in pairs of nonidentical dynamics.

DOI: [10.1103/PhysRevE.95.012210](https://doi.org/10.1103/PhysRevE.95.012210)

I. INTRODUCTION

The characterization of interdependence between interacting dynamics is important for the understanding of the behavior of many real-world systems. Prominent examples include the stock market [1,2], the cardiorespiratory system [3,4], the brain [5,6], or the climate [7,8]. In general, the interacting dynamics are nonidentical. This raises the question: Is it possible to define a symmetric interaction between nonidentical coupled dynamics? To address this question, we use a data-driven approach by analyzing pairs of signals derived from coupled model systems. For this type of analysis, in the bivariate or multivariate case, a variety of different approaches has been proposed. Among them are approaches based on state-space reconstruction [9–14], phases [15–21], information theory [22–27], linear correlation [28–30], dynamical Bayesian inference analysis [31–35], as well as on neural networks [36,37], among others. A comparison between many of these approaches was done in model systems and also in experimental data [21,35,38–42]. In this study we apply a state-space approach [14] and a phase-based approach [15,18,19].

We consider two bidirectionally coupled dynamics X and Y , the evolution of which is described by the time-dependent state-space vectors $\mathbf{x}(t) = \{x_1(t), x_2(t), \dots, x_k(t)\}$ and $\mathbf{y}(t) = \{y_1(t), y_2(t), \dots, y_l(t)\}$, respectively. Their equations of motion have the form

$$\begin{aligned}\dot{\mathbf{x}}(t) &= F(\mathbf{x}(t), f(y_i(t), x_j(t), \epsilon_y)), \\ \dot{\mathbf{y}}(t) &= G(\mathbf{y}(t), g(x_j(t), y_i(t), \epsilon_x)).\end{aligned}\quad (1)$$

The function f represents an interaction from the Y to the X dynamics with coupling strength ϵ_y . The y_i and x_j components are involved in this interaction, with $j = 1, \dots, k$ and $i = 1, \dots, l$. Analogously, the function g represents the interaction from the X to the Y dynamics with coupling strength ϵ_x .

Rosenblum and Pikovsky [15] applied a directional phase-based approach in a system of bidirectionally coupled dynamics X and Y . They found that when the coupled dynamics X and Y are almost identical, equal estimates of the interdependence in both directions, as judged by their phase-based approach, were correctly obtained for equal ϵ_x, ϵ_y values. On the other hand, they indicated that when the X and Y dynamics are nonidentical, equal estimates of the interdependence in both directions are obtained for different ϵ_x, ϵ_y values.

To address this asymmetry in coupled dynamics we introduce the notion of coupling impact. The coupling impact takes into account both the coupling strength and the energy of the individual dynamics. As a data-driven estimator of this energy we use the variance of the signals. In particular we use the variance of the variables through which the dynamics are coupled. This is straightforward, since it is this variance in combination with the coupling strength that reflects the energy that is transmitted from one dynamics to the other. In order to characterize the interdependence among the bidirectionally coupled dynamics we use the directional state-space measure L introduced by Chicharro and Andrzejak [14] and the phase-based directionality index $d_{x,y}$ introduced by Rosenblum and Pikovsky [15,18,19]. We determine the coupling strength values as well as the coupling impact values for which the two directional connectivity measures L and $d_{x,y}$ judge the interaction to be symmetric. First, we explain the measures L and $d_{x,y}$ (Secs. II A and II B) and present the coupled dynamics (Sec. II C). In Sec. II D, we introduce the coupling impact, and the results are shown in Sec. III. Finally, in Sec. IV we discuss the conclusions of this study.

II. METHODS

In this section we present the two approaches that we use for the characterization of directional interdependence between two coupled dynamics X and Y . The first one is

based on the state-space reconstruction and is denoted by L [14], while the second one is based on the reconstruction of the phase dynamics and is denoted by $d_{x,y}$ [15,18,19]. The state-space approach utilizes directly the measured amplitudes to reconstruct an estimator of the attractor of the underlying dynamics using delay coordinates. This is based on the assumption that the particular measured signal reflects all the degrees of freedom of the dynamics. Furthermore, it requires the dynamics to be aperiodic. For the phase-based approach, techniques such as the Hilbert transform are used to extract phases from the amplitudes of the signals. This approach is based on the assumption that the dynamics can be described by a phase variable and this phase variable can be reconstructed from the signal [43]. Moreover, it is assumed that the interacting dynamics X and Y are self-sustained. For both approaches, strong coupling between X and Y should not be present. When two dynamics are synchronized in the phase or in the amplitude domain then the detection of the interaction direction is no longer possible [14,15,24–26,39]. Additionally, in both approaches we assume stationarity in the sense that the generating dynamics has no explicit time dependence. In the first part of our analysis we investigate chaotic dynamics. For most of these particular dynamics phases are not well-defined. Thus, we analyze them using the state-space approach. We furthermore study noisy-limit cycle oscillators. Since here phases are well-defined we use the phase-based approach.

A. State-space approach

The state-space approach L [14] is a bivariate directional interdependence measure and it belongs to the category of the nonlinear state-space measures. After reconstruction of the state-space of the dynamics, the measure L quantifies the degree to which spatially close neighbors of one dynamics are mapped to spatially close neighbors on the other dynamics. It was successfully applied to experimental data, like neuronal [44] and musical data [45]. Moreover, in combination with surrogates it was applied to electroencephalographic recordings from epilepsy patients and it was shown that it is able to localize the epileptic focus [46] as well as to assess the nonlinear interdependence in the brain [47].

We now review the algorithm [14] for the calculation of $L(X|Y)$ and $L(Y|X)$, which are used to estimate the interdependence from $X \rightarrow Y$ and $Y \rightarrow X$, respectively. Suppose that we have two simultaneously measured signals $x_i, y_i, i = 1, \dots, N$ derived from the dynamics X and Y , respectively. Using the method of delays [48], we reconstruct the X and Y dynamics with embedding delay τ and embedding dimension m . The embedding vectors for the X dynamics are $\mathbf{x}_n = (x_n, x_{n-\tau}, \dots, x_{n-(m-1)\tau})$ and for the Y dynamics they are $\mathbf{y}_n = (y_n, y_{n-\tau}, \dots, y_{n-(m-1)\tau})$, where $n = h + 1, \dots, N$ and $h = (m - 1)\tau$.

To calculate $L(X|Y)$, we start with a nearest-neighbor search in the X dynamics. For each reference embedding vector \mathbf{x}_i we calculate its squared Euclidean distance $d(\mathbf{x}_i, \mathbf{x}_o)$ from all the other embedding vectors $\mathbf{x}_o, o = h + 1, \dots, N, i \neq o$. With $u_{i,j}, j = 1, \dots, k$, we denote the time indices of the k spatially nearest neighbors of the reference embedding vector \mathbf{x}_i . In order to avoid the selection of temporally close neighbors, we apply a Theiler window, W [49]. This means

that the time indices of all neighbors of \mathbf{x}_i should satisfy $|u_{i,j} - i| > W$. We perform the same steps for the Y dynamics and with $w_{i,j}, j = 1, \dots, k$ we denote the time indices of the k nearest neighbors of each reference embedding vector \mathbf{y}_i . Finally, for each reference point of the X dynamics, \mathbf{x}_i , we calculate the Y -conditioned mean rank $G_i^k(X|Y) = \frac{1}{k} \sum_{j=1}^k g_{i,w_{i,j}}$. The term $g_{i,w_{i,j}}$ denotes the rank that the distance $d(\mathbf{x}_i, \mathbf{x}_{w_{i,j}})$ takes in a sorted ascending list of all the distances $\{d(\mathbf{x}_i, \mathbf{x}_o)\}, o = h + 1, \dots, N$ and $i \neq o$.

$L(X|Y)$ is defined by

$$L(X|Y) = \frac{1}{N - h} \sum_{i=h+1}^N \frac{G_i(X) - G_i^k(X|Y)}{G_i(X) - G^k(X)}. \quad (2)$$

The term $G^k(X) = \frac{k+1}{2}$ is a constant and denotes the mean value of the ranks of the k nearest neighbors of each reference point \mathbf{x}_i . Furthermore, we have $G_i(X) = (M_i + 1)/2$, where $M_i = N - 2W - 1$ holds for the range $W < i < N - W + 1$. Below and above the bounds of this range M_i increases linearly and reaches $M_i = N - W - 1$ at $i = 1$ and $i = N$.

When we have identical synchronization ($Y = X$) then $G_i^k(X|Y) = G^k(X)$, and $L(X|Y) = 1$. If there is an interaction from $X \rightarrow Y$ then $0 < L(X|Y) < 1$. When the dynamics X and Y are independent, then $G_i^k(X|Y) \approx G_i(X)$ and the values of $L(X|Y)$ are distributed symmetrically around zero. To assess the interdependence $L(Y|X)$ from Y to X we follow the above process by exchanging the roles of X and Y . Accordingly, we define $\Delta L = L(X|Y) - L(Y|X)$ for the characterization of the predominant direction of interaction between the X and Y dynamics [50].

In a preanalysis we scanned the ranges $k = [3, 5, 10, 15, 20]$, $m = [4, 5, 6, 7, 8, 9]$, and $\tau = [4, 5, 6, 7, 8, 9]$ sampling times. For all the possible combinations between k, m , and τ the values of ΔL were stable for $k = [3, 5, 10]$, $m = [4, 5, 6]$, and $\tau = [4, 5, 6]$. Therefore, without performing any kind of optimization, we set the values of k, m , and τ to the middle value of these ranges. In other words, we set the parameters of L : $k = 5$ nearest neighbors, embedding dimension $m = 5$ and embedding delay $\tau = 5$ sampling times. For the Theiler window we use $W = 15$. Like described below in more detail, we sample all our dynamics such they have approximately 20 samples per cycle. Accordingly, for the parameters τ and W , which are in units of time, we can use the same values across all dynamics.

B. Phase-based approach

The bivariate directional phase-based approach $d_{x,y}$ [15,18,19] aims at the reconstruction of pairs of coupled phase dynamics through an analysis of the instantaneous phases and the instantaneous frequencies. Later, it was extended to characterize interactions in networks of coupled oscillators [20,21]. It was successfully applied not only in bivariate but also in multivariate model systems and experimental data [4,15,18–21,51–54].

This approach is based on the fact that an autonomous periodic oscillator can be characterized by a phase ϕ , which grows uniformly in time,

$$\dot{\phi} = \omega, \quad (3)$$

where ω is the natural frequency and the dot denotes the time-derivative. For the case of two coupled dynamics X, Y we have to take into account their interaction. Accordingly, they can be described

$$\begin{aligned}\dot{\phi}_x &= \omega_x + q_x(\phi_x, \phi_y), \\ \dot{\phi}_y &= \omega_y + q_y(\phi_y, \phi_x),\end{aligned}\quad (4)$$

where $\phi_{x,y}$ are the phase variables, $\omega_{x,y}$ govern the natural frequencies, and $q_{x,y}$ are the coupling functions which are 2π -periodic with respect to their arguments [15,43]. The interaction between the X and Y dynamics can be quantified with the norms of the coupling functions $q_{x,y}$. The interaction from $Y \rightarrow X$ and viceversa can be characterized by $c_x = \frac{\|q_x\|}{\omega_x}$ and $c_y = \frac{\|q_y\|}{\omega_y}$, respectively. Finally, the directionality index $d_{x,y}$ [15] is calculated as

$$d_{x,y} = \frac{c_y - c_x}{c_x + c_y}. \quad (5)$$

For uncoupled dynamics, zero values of $d_{x,y}$ are expected. With increasing unidirectional coupling from X to Y , positive values of $d_{x,y}$ with an upper bound of 1 are obtained. For the opposite coupling direction, negative values are attained with a limit of -1 . The sign of $d_{x,y}$ can be used to conclude the predominant coupling direction. Additionally, equal estimates of interaction in both directions between X and Y result in zero values of $d_{x,y}$. When we want to assess the interdependence in real-world dynamics we only have measurements while the frequencies and the coupling functions of the phase dynamics [Eqs. (4)] are unknown. Therefore, we have to reconstruct the phase dynamics. If the measurements are given by some amplitude variables the first step of this approach is to obtain phases from the available measurements. This process is done in two stages. First, we extract with a two-dimensional embedding, e.g., the analytic signal approach based on the Hilbert transform cyclic variables θ , which are called protophases [18,19]. For any autonomous dynamics protophases do not, in general, grow linearly in time but they follow $\dot{\theta} = f(\theta)$. Moreover, they are 2π -periodic and they depend on the embedding method. Therefore, the second stage is to obtain the genuine phases ϕ of Eq. (3) through a transformation from $\theta \rightarrow \phi$. This transformation is invertible and it is neither an interpolation nor a filtering [18,19]. After obtaining the genuine phases we numerically calculate their time derivatives. According to Eq. (4) the derivatives of the phases are 2π -periodic functions of the phases. Hence, we represent the right-hand side of Eq. (4) as double Fourier series of order p :

$$\begin{aligned}\dot{\phi}_{x,y} &= \omega_{x,y} + q_{x,y}(\phi_x, \phi_y) + \xi_{x,y} \\ &= \sum_{m=-p}^p \sum_{l=-p}^p Q_{m,l}^{(x,y)} e^{i(m\phi_x + l\phi_y)} + \xi_{x,y}.\end{aligned}$$

Here, we include noise terms $\xi_{x,y}$ that are always present in real-world data. The coefficients $Q_{m,l}^{(x,y)}$ are estimated by means of a least-mean-square fit. From the coefficients $Q_{0,0}^{(x,y)}$ we estimate the natural frequencies $\omega_{x,y}$ that are denoted by $\bar{\omega}_{x,y}$ [18,19]. The norms of the coupling functions are given

by

$$N^{(x,y)} = \left(\sum_{m=-p}^p \sum_{l=-p}^p |Q_{m,l}^{(x,y)}|^2 \right)^{1/2}. \quad (6)$$

From the summation and for both X and Y dynamics the case for which $m = l = 0$ (estimated natural frequencies) is excluded. In the end the norms $N^{(x,y)}$ of the coupling functions are normalized by the estimated natural frequencies in order to obtain the influence of one dynamics on the other,

$$c_x = \frac{N^{(x)}}{\bar{\omega}_x}, \quad c_y = \frac{N^{(y)}}{\bar{\omega}_y}. \quad (7)$$

Finally, by substituting Eqs. (7) in Eq. (5) we obtain the directionality index $d_{x,y}$ [55].

We use the source code resources of Ref. [55] to obtain the directionality index. Particularly, we use the Hilbert transform to obtain the protophases. We make the transformation from protophases to phases with the optimization according to Tenreiro [56]. For the calculation of the derivatives of the genuine phases we use the central finite difference. Furthermore, the order p of the Fourier expansion is 10. For the calculation of the norms of the coupling functions we use the trapezoidal method [55].

C. Coupled dynamics

We analyze pairs of bidirectionally coupled deterministic chaotic dynamics as well as noisy limit-cycle oscillators. The pairs of chaotic dynamics comprise identical, almost identical, and nonidentical coupled Lorenz, Rössler, and Rössler-Lorenz dynamics. We also use noisy nonidentical van der Pol oscillators as an example of limit-cycle oscillators. As we mentioned before (Sec. II), we want to avoid synchronization between the X and Y dynamics. Therefore, we restrict our analysis to coupling strength values that do not result in a functional relation between the amplitudes (for the chaotic dynamics) and between the phases (for the limit-cycle oscillators). Without loss of generality, we fix the coupling strength from X to Y , denoted by ϵ_x , and we vary the coupling strength from Y to X , denoted by ϵ_y . Our first dynamics are coupled Lorenz:

$$\begin{aligned}\dot{x}_1(t) &= 10[-x_1(t) + x_2(t)] + \epsilon_y [y_1(t) - x_1(t)], \\ \dot{x}_2(t) &= R_x x_1(t) - x_2(t) - x_1(t) x_3(t), \\ \dot{x}_3(t) &= x_1(t) x_2(t) - \frac{8}{3} x_3(t),\end{aligned}\quad (8)$$

and

$$\begin{aligned}\dot{y}_1(t) &= 10[-y_1(t) + y_2(t)] + \epsilon_x [x_1(t) - y_1(t)], \\ \dot{y}_2(t) &= R_y y_1(t) - y_2(t) - y_1(t) y_3(t), \\ \dot{y}_3(t) &= y_1(t) y_2(t) - \frac{8}{3} y_3(t).\end{aligned}\quad (9)$$

Here, the coupling strength from $X \rightarrow Y$ is fixed to $\epsilon_x = 1.2$ and the coupling strength ϵ_y from $Y \rightarrow X$ runs from 0.5 to 2.48 in steps of 0.02. All dynamics depend on some parameters. Therefore, we can control the degree of asymmetry between the dynamics by changing these parameters. For the coupled Lorenz dynamics, we vary the values of R_x, R_y from 48 to 54 in steps of 2. Taking all the possible combinations of

R_x, R_y values we obtain 12 pairs of nonidentical and 4 pairs of identical coupled Lorenz dynamics. We analyze the signals that are obtained from the components x_1, y_1 .

For the integration of all chaotic dynamics we use the fourth-order Runge-Kutta method. For the coupled Lorenz dynamics [Eqs. (8) and (9)], the step size for the integration is 0.005 time units and the sampling interval is $\Delta t = 0.03$ time units. As a consequence, every rotation period of the Lorenz dynamics contains approximately 20 samples, which we consider as an appropriate sampling of the dynamics [39]. We always use random initial conditions and in order to discard transients we apply preiterations in the numerical integration. The signals that we use for the analysis consist of 4096 points and they correspond to 200 basic periods approximately.

For the coupled Rössler dynamics [57] the equations read

$$\begin{aligned}\dot{x}_1(t) &= -\omega_x x_2(t) - x_3(t) + \epsilon_y [y_1(t) - x_1(t)], \\ \dot{x}_2(t) &= \omega_x x_1(t) + 0.25 x_2(t), \\ \dot{x}_3(t) &= (x_1(t) - 8.5) x_3(t) + 0.4,\end{aligned}\quad (10)$$

and

$$\begin{aligned}\dot{y}_1(t) &= -\omega_y y_2(t) - y_3(t) + \epsilon_x [x_1(t) - y_1(t)], \\ \dot{y}_2(t) &= \omega_y y_1(t) + 0.25 y_2(t), \\ \dot{y}_3(t) &= (y_1(t) - 8.5) y_3(t) + 0.4.\end{aligned}\quad (11)$$

The mean frequencies ω_x, ω_y take the values $\omega_x, \omega_y = \{0.9, 0.905, 1.045, 1.05\}$. Thus, the 16 possible combinations between the ω_x, ω_y values can be classified as follows. We obtain four pairs of identical (e.g., $\omega_x = 0.9, \omega_y = 0.9$), four pairs of almost identical (e.g., $\omega_x = 0.9, \omega_y = 0.905$) and eight pairs of nonidentical coupled Rössler dynamics (e.g., $\omega_x = 0.9, \omega_y = 1.05$). We fix $\epsilon_x = 0.02$ and the ϵ_y values run from 0.01 to 0.0298 in steps of 0.0002. The integration step is 0.05 time units, and the sampling interval is set to $\Delta t = 0.3$ time units, again resulting in approximately 20 points per cycle. We use the variables x_1, y_1 as observables.

We also study the Rössler-Lorenz dynamics an example where the dynamics do not only have different parameters but they also have different structure:

$$\begin{aligned}\dot{x}_1(t) &= 10[-\omega_x x_2(t) - x_3(t)] + \epsilon_y [y_2(t) - x_1(t)], \\ \dot{x}_2(t) &= 10[\omega_x x_1(t) + 0.25 x_2(t)], \\ \dot{x}_3(t) &= 10\{[x_1(t) - 8.5] x_3(t) + 0.4\},\end{aligned}\quad (12)$$

and

$$\begin{aligned}\dot{y}_1(t) &= 10[-y_1(t) + y_2(t)], \\ \dot{y}_2(t) &= R_y y_1(t) - y_2(t) - y_1(t) y_3(t) + \epsilon_x [x_1(t) - y_2(t)], \\ \dot{y}_3(t) &= y_1(t) y_2(t) - \frac{8}{3} y_3(t).\end{aligned}\quad (13)$$

We vary the ω_x values as well as the R_y values in the same ranges that we used for the coupled Rössler and coupled Lorenz dynamics, namely $\omega_x = \{0.9, 0.905, 1.045, 1.05\}$ and $R_y = \{48, 50, 52, 54\}$. Therefore, across all the combinations of ω_x and R_y we obtain 16 pairs of coupled Rössler-Lorenz dynamics. The fixed coupling strength from X to Y is $\epsilon_x = 0.55$ and the varied coupling strength from Y to X is $\epsilon_y = 0.3/1.02^{i-1}$, $i = 1, \dots, 100$. The step size for the integration is 0.005 time units and the sampling interval is

$\Delta t = 0.03$ time units. Since we use the same Rössler and Lorenz dynamics as in the previous coupled dynamics, we multiply the right-hand side of the Rössler equations with the factor of 10 to continue to have approximately 20 points per cycle for both dynamics. In this dynamics we analyzed the signals from the x_1, y_2 components.

The limit-cycle oscillators consist of van der Pol oscillators which read

$$\begin{aligned}\ddot{x}(t) &= 0.2[1 - x^2(t)]\dot{x}(t) - \omega_x^2 x(t) + \epsilon_y [y(t) - x(t)] + \eta_x, \\ \ddot{y}(t) &= 0.2[1 - y^2(t)]\dot{y}(t) - \omega_y^2 y(t) + \epsilon_x [x(t) - y(t)] + \eta_y,\end{aligned}\quad (14)$$

where η_x, η_y are independent white Gaussian noises with zero mean and correlation functions $\langle \eta_{x,y}(t) \eta_{x,y}(t') \rangle = 2D_{x,y} \delta(t - t')$. For the integration of this type of dynamics we use the Euler method with step size $dt = 0.01\pi$ time units. The variables x, y are used as observables. The sampling interval is 0.1π time units again resulting in approximately 20 points per cycle for each oscillator. The values of the frequencies ω_x, ω_y vary in steps of 0.01 in the ranges $[1.09, 1.12]$ and $[0.88, 0.91]$, respectively. Accordingly, we obtain 16 pairs of nonidentical coupled oscillators. For the aforementioned ranges of frequency we fix the standard deviation of noise, the so-called noise level $\xi_{x,y} = \sqrt{2D_{x,y}}$ to 0.04. We also vary the values of $\xi_{x,y}$ in the range $[0.02, 0.05]$ in steps of 0.01, while the frequencies are fixed to $\omega_x = 1.1$ and $\omega_y = 0.9$. Concerning the coupling values, ϵ_x is set to 0.05, and the ϵ_y values vary in steps of 2×10^{-4} in the range $[0.04002, 0.06]$. Like for the chaotic dynamics we limit the range of the coupling values such that we do not have synchronization. A study of the effect of the coupling strength and noise on synchronization can be found in Ref. [58].

D. Coupling impact

The relevant components in a bidirectional interaction between two coupled dynamics are the coupling strengths as well as the variables of the dynamics, which are contained in the coupling terms. For diffusively coupled dynamics X and Y that are identical (or almost identical), these variables are the same (or almost the same). Thus, symmetric interactions between X and Y can be defined directly from the coupling strengths. On the other hand, when X and Y are nonidentical the variables that are contained in the coupling terms are different. Hence, the coupling strengths are not by themselves sufficient to characterize an interaction to be symmetric. Instead, in order to define a symmetric interaction between X and Y we also have to consider the energy of the variables through which the coupling is conveyed from one dynamics to the other.

In this paper we propose the notion of the coupling impact as a quantity that takes into account both the coupling strengths and the variables' energy. As a data-driven estimator of the variables' energy we use the variance of their corresponding signals. Accordingly, the coupling impact γ_x from X to Y dynamics is given by

$$\gamma_x = \frac{\epsilon_x}{\sigma_y^2}, \quad (15)$$

where ϵ_x is the coupling strength from $X \rightarrow Y$ and σ_y^2 is the variance of the signal that corresponds to the variable of the Y dynamics, which is contained on the coupling term. For the coupling impact γ_y of the other direction $Y \rightarrow X$, we exchange the roles of the x and y components in Eq. (15).

What is the relation between the values of the coupling strength and between the values of the coupling impact when there is a symmetric interaction in the coupled X and Y dynamics as estimated by L or $d_{x,y}$? In other words, what is the relation between the ϵ_x, ϵ_y values as well as the one between the γ_x, γ_y values for which we obtain $\Delta L = 0$ or $d_{x,y} = 0$?

We carry out an analysis in two stages. We start by describing the process we follow for the chaotic dynamics that we analyze with the measure $\Delta L = L(X|Y) - L(Y|X)$. At first, we pair the fixed value of the coupling strength ϵ_x with a range of 100 values of ϵ_y . The exact range of ϵ_y is determined in a preanalysis such that in its intermediate range, and given ϵ_x , we obtain equality in the values of L in both directions [Fig. 1(a)]. For each pair of dynamics and for each of the 100 sets of the coupling strength (ϵ_x, ϵ_y) we generate 500 independent realizations. In Fig. 1(b) we show the mean values of ΔL across the 500 realizations in dependence on the ratio $r_\epsilon = \epsilon_y/\epsilon_x$ of the coupling strength values. As a consequence of the adjustment of the ϵ_y range, the curve of ΔL crosses zero. In order to estimate the abscissa of the zero-crossing point ($\Delta L = 0$), we fit a third-order polynomial on the curve of the mean values of ΔL using the Brent-Dekker method [59]. The resulting abscissa value is denoted by $r_{\epsilon 0}$. In other words, $r_{\epsilon 0}$ is the approximated value of ϵ_y/ϵ_x for which there is a symmetric interaction between the X and Y dynamics as judged by the measure L . We illustrate the second stage of our analysis in Fig. 1(c). We plot the mean values of the measure ΔL not in dependence on the ratio of the coupling strength values $r_\epsilon = \epsilon_y/\epsilon_x$, but in dependence on the ratio of the coupling impact values $r_\gamma = \gamma_y/\gamma_x$. We denote by $r_{\gamma 0}$ the abscissa of the point for which we have $\Delta L = 0$. Similarly, for the limit-cycle oscillators we follow exactly the same process, but instead of ΔL we use the directionality index $d_{x,y} = (c_y - c_x)/(c_x + c_y)$.

If we get $r_{\epsilon 0} = 1$ this would mean that equal estimates of the interaction between the X and Y dynamics as judged by the measure ΔL (or $d_{x,y}$) are obtained for equal coupling strength values. Analogously, $r_{\gamma 0} = 1$ means that symmetric interaction in the coupled X and Y dynamics is obtained for equal coupling impact values. In order to quantify deviations of $r_{\epsilon 0}$ and $r_{\gamma 0}$ from one, we define the quantities $\rho_\epsilon = \ln(r_{\epsilon 0})$ and $\rho_\gamma = \ln(r_{\gamma 0})$.

III. RESULTS

We start by illustrating the influence of the asymmetry between the dynamics and the coupling on the variances of the signals. We do this since the variance is the basic component of the coupling impact values. Thus, we inspect the relation between the ratio of the coupling strength values $r_\epsilon = \epsilon_y/\epsilon_x$ and the ratio of the variance of the signals $r_v = \sigma_y^2/\sigma_x^2$ across different pairs of Lorenz dynamics (Fig. 2). For coupled identical dynamics with equal coupling strength values ($r_\epsilon = 1$), the r_v ratio is 1, correctly reflecting the symmetry of the dynamics and the coupling. For increasingly

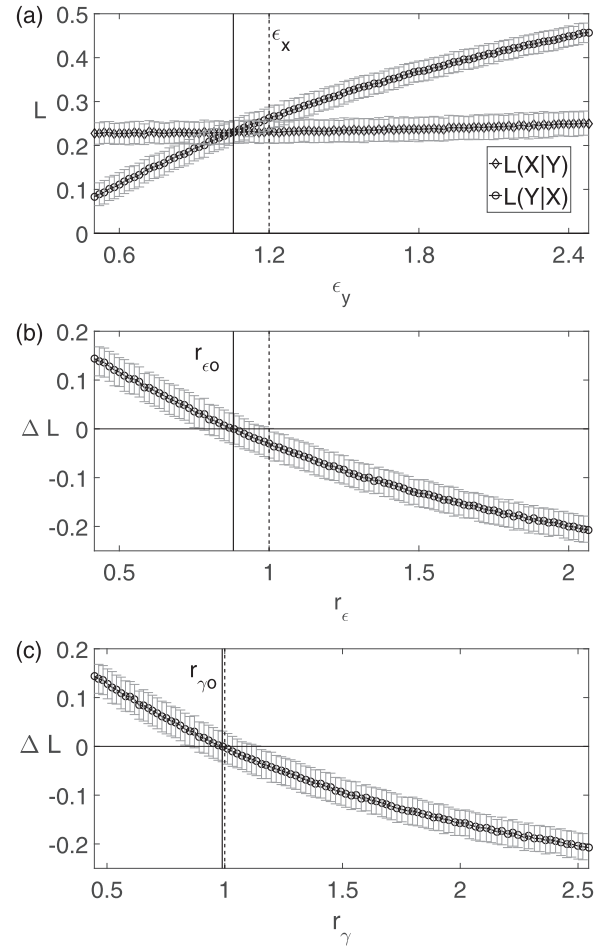


FIG. 1. The coupling impact but not the coupling strength detects a symmetric interaction in strongly asymmetric coupled Lorenz dynamics. Values of L and ΔL for the coupled Lorenz dynamics ($R_x = 48$, $R_y = 54$). The error bars depict the mean \pm one standard deviation across 500 independent realizations. In (a) we depict values of $L(X|Y)$, $L(Y|X)$ in dependence on the coupling strength ϵ_y . The vertical dashed line marks the fixed coupling strength $\epsilon_x = 1.2$ from $X \rightarrow Y$. In (b) the $\Delta L = L(X|Y) - L(Y|X)$ values are shown in dependence on the ratio of the coupling strength values $r_\epsilon = \epsilon_y/\epsilon_x$. Panel (c) shows the ΔL values in dependence on the ratio of the coupling impact values $r_\gamma = \gamma_y/\gamma_x$. In panels (b) and (c) the dashed vertical lines highlight the abscissa value of one. The black solid line in (a) marks the crossing point of $L(X|Y)$, $L(Y|X)$ in (b) the solid line stands for the $r_{\epsilon 0}$ value and in (c) for the $r_{\gamma 0}$ value.

nonidentical dynamics, the r_v ratio gradually diverges from the one obtained for identical dynamics. In addition, for any degree of asymmetry between the dynamics, r_v covaries with r_ϵ .

We now consider strongly asymmetric coupled Lorenz dynamics [Eqs. (8) and (9) for $R_x = 48$, $R_y = 54$]. The coupling strength ϵ_x from $X \rightarrow Y$ dynamics is fixed. As a consequence the values of $L(X|Y)$ form an almost horizontal line [Fig. 1(a)]. In contrast, since the ϵ_y coupling strength from Y to X dynamics is increasing, so do the values of $L(Y|X)$ [Fig. 1(a)]. The graphs in Fig. 1(b) and Fig. 1(c) show the resulting $\Delta L = 0$ values. In each panel, however, the abscissa is scaled differently. We use ϵ_y in Fig. 1(a), r_ϵ in Fig. 1(b), and r_γ in Fig. 1(c). Nonetheless, by construction, the crossing

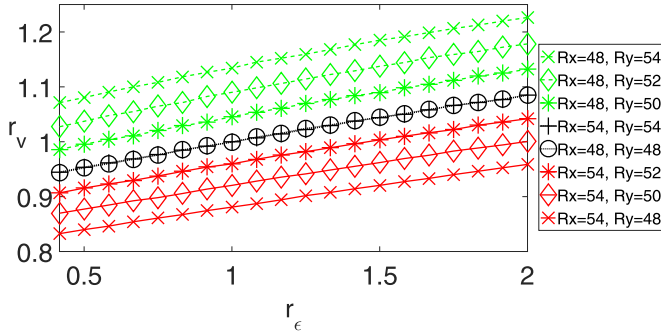


FIG. 2. Both the asymmetry and the coupling strength of the dynamics affect the variance of the signals. Mean values of the ratio of the variances of the signals $r_v = \sigma_y^2/\sigma_x^2$ in dependence on the ratio of the coupling strength values $r_\epsilon = \epsilon_y/\epsilon_x$. Each curve corresponds to a different coupled Lorenz dynamics with the R_x and R_y values specified in the legend.

point of $L(X|Y)$ and $L(Y|X)$ in Fig. 1(a) and the zero crossing of $\Delta L = 0$ in Figs. 1(b) and 1(c) all have approximately the same relative position with regard to the abscissa limits. These lines are all positioned in the 29th data point. However, in Fig. 1(c) the distance between pairs of subsequent points is not constant but depends on the ratio of variances. The ratio of variances in turn depends on the ϵ_y (see again Fig. 1).

When the degree of interdependence is the same in both directions, as judged by $\Delta L = 0$, the corresponding ratio $r_{\epsilon o}$ of the coupling strength values is different from 1 [Fig. 1(b)]. On the other hand, when we use the ratio r_γ of the coupling impact

values, for $\Delta L = 0$ the $r_{\gamma o}$ value is almost equal to 1 [Fig. 1(c)]. This means that equal estimates of interdependence ($\Delta L = 0$) are obtained for unequal coupling strength values ($r_{\epsilon o} \neq 1$), but for almost equal coupling impact values ($r_{\gamma o} \approx 1$).

We now turn to the effect of the degree of asymmetry of the coupled dynamics on the quantities $\rho_\epsilon = \ln(r_{\epsilon o})$ and $\rho_\gamma = \ln(r_{\gamma o})$ (Fig. 3). We start with the coupled Lorenz dynamics [Eqs. (8) and (9) for all the set of R_x, R_y values]. For pairs of identical dynamics we obtain zero values of ρ_ϵ [Fig. 3(a)]. In contrast, for pairs of nonidentical dynamics we obtain nonzero values of ρ_ϵ . We also find that an increase in the asymmetry of the dynamics leads to an increase in the absolute values of ρ_ϵ [Fig. 3(a)]. In contrast, the use of coupling impact renders the resulting values of ρ_γ to be almost zero for both identical and nonidentical bidirectionally coupled Lorenz dynamics [Fig. 3(d)]. Similar findings are obtained for the coupled Rössler dynamics [Eqs. (10) and (11) for all the set of ω_x, ω_y values] as can be seen in Figs. 3(b) and 3(e). Again we find that zero values of ρ_ϵ and ρ_γ are obtained for all the pairs of identical dynamics. These results also hold for pairs of almost identical dynamics [top left and bottom right blocks of Figs. 3(b) and 3(e)]. Concerning the pairs of nonidentical dynamics we obtain nonzero values of ρ_ϵ [Fig. 3(b)]. On the other hand, the values of ρ_γ are almost zero [Fig. 3(e)].

We continue with an example of coupled dynamics with different structure given by the Rössler and Lorenz dynamics [Eqs. (12) and (13)]. Since these dynamics are completely different, the ρ_ϵ quantity takes nonzero values [Fig. 3(c)] for all the pairs of dynamics. Moreover, these values are higher than the ones of the coupled Lorenz [Fig. 3(a)] and Rössler dynamics [Fig. 3(b)]. Despite the strong asymmetry between

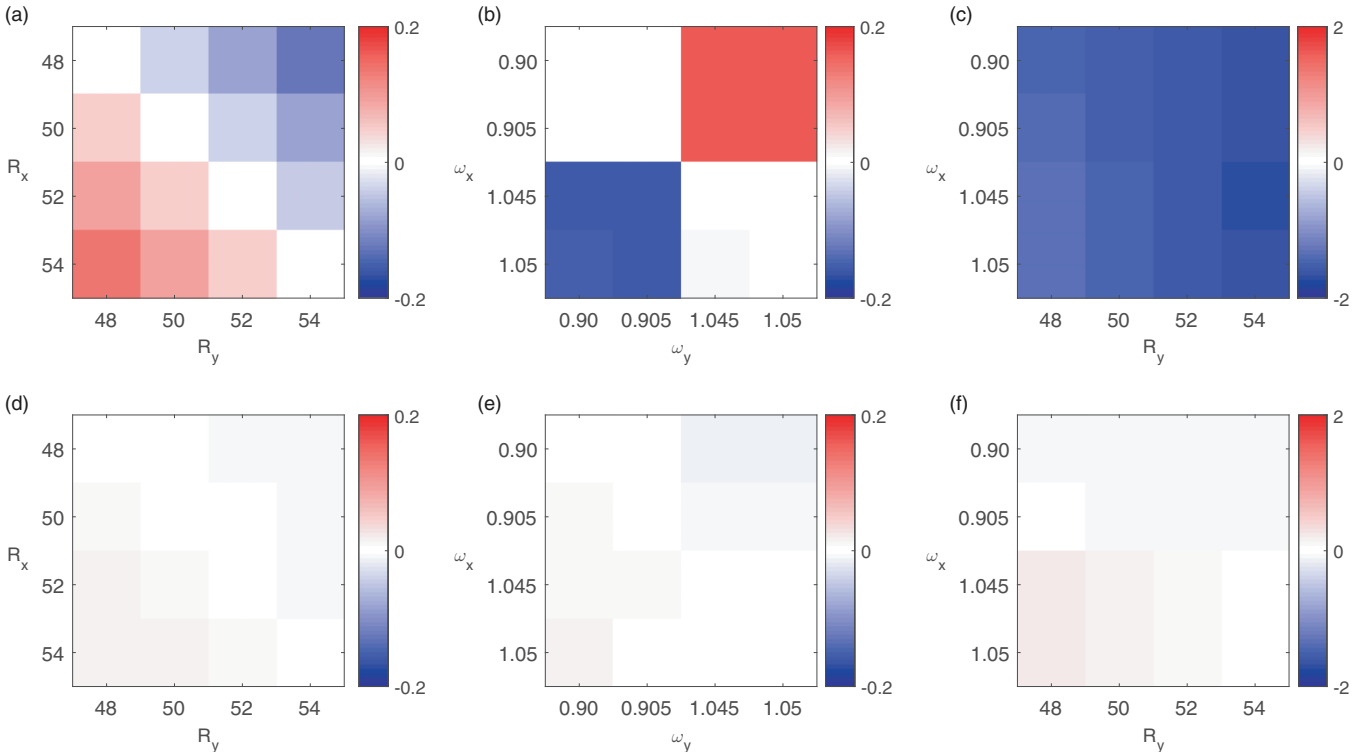


FIG. 3. The coupling impact correctly detects a symmetric interaction for the coupled deterministic chaotic dynamics. Values of ρ_ϵ (a–c) and ρ_γ (d–f) for the coupled Lorenz (a, d), Rössler (b, e), and Rössler-Lorenz (c, f) dynamics.

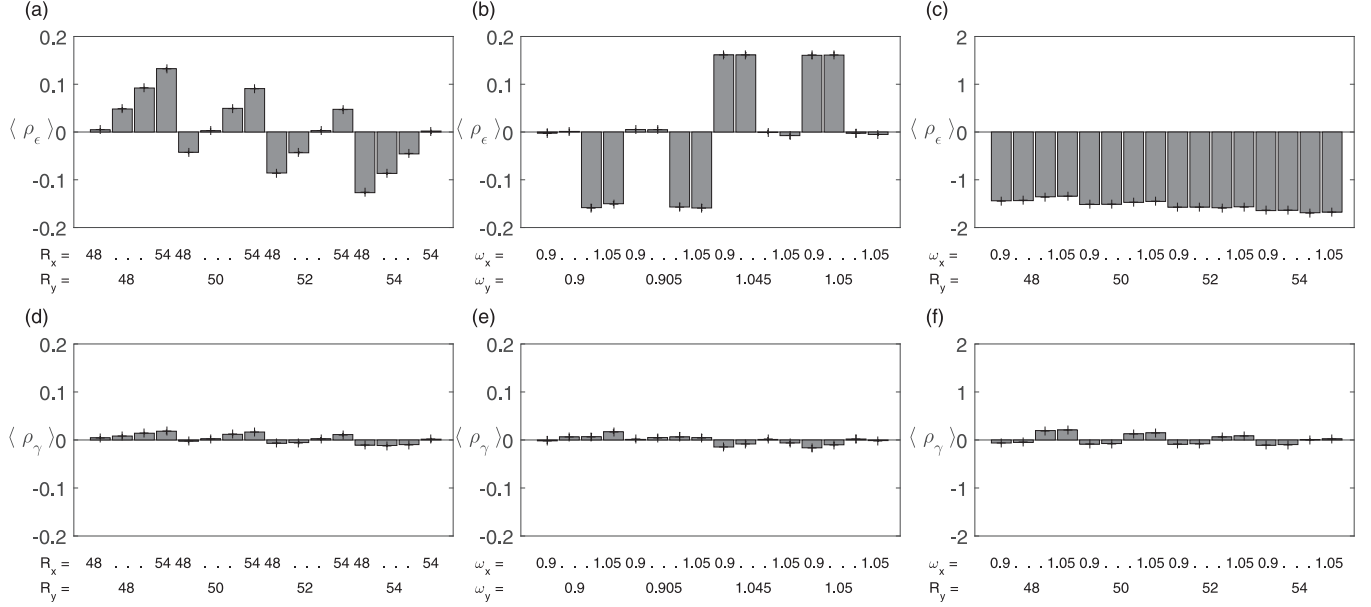


FIG. 4. High accuracy of the estimation of the coupling strength and coupling impact values. Mean values of ρ_ϵ (a–c) and ρ_γ (d–f) for the coupled Lorenz (a, d), Rössler (b, e), and Rössler-Lorenz (c, f) dynamics obtained across five sets of 100 realizations each. The error bars depict the corresponding ranges.

the coupled dynamics the use of coupling impact successfully results in values of ρ_γ that are very close to zero [Fig. 3(f)].

In order to assess the accuracy of our results we divide the 500 independent realizations that we made for each pair of dynamics in 5 groups of 100 realizations each. For every group we repeat the analysis as described in Sec. II D and we determine the corresponding ρ_ϵ and ρ_γ values. Their mean value and ranges are shown in Fig. 4. The small magnitude of these ranges illustrates that our estimates of ρ_ϵ and ρ_γ are reliable.

We now study limit-cycle oscillators. We follow the exact same procedure like the first three chaotic dynamics, but instead of the measure L we use the directionality index $d_{x,y}$. In particular, we assure that the estimates ρ_ϵ and ρ_γ are of comparably high accuracy as the one obtained for the chaotic dynamics. For all the pairs of nonidentical van der Pol oscillators [Eqs. (14) with $\xi_{x,y} = 0.04$] the values of ρ_ϵ diverge from zero [Fig. 5(a)]. Again the more asymmetry between the frequencies ω_x, ω_y of the oscillators the higher absolute values of ρ_ϵ we get. In contrast, the use of coupling impact results in values of ρ_γ close to zero [Fig. 5(c)]. We also study the role of noise on the coupling impact. For this purpose, we fix $\omega_x = 1.1, \omega_y = 0.9$ and we vary the noise levels ξ_x, ξ_y from 0.02 to 0.05 in steps of 0.01. In general higher values of noise lead to higher absolute values of ρ_ϵ [Fig. 5(b)]. On contrary, the use of coupling impact ends in values of ρ_γ very close to zero [Fig. 5(d)].

IV. DISCUSSION

In this paper we proposed the notion of the coupling impact as a way to define symmetric interactions between nonidentical bidirectionally coupled dynamics. For this purpose we followed a data-driven approach by analyzing signals from pairs of coupled dynamics. In order to characterize the interdependence between the interacting dynamics we used the state-space measure L [14] as well as the phase-based

directionality index $d_{x,y}$ [15,18,19]. These measures estimate the strength and direction of the interaction between two dynamics X and Y . At first, we showed that in identical and almost identical bidirectionally coupled dynamics, equal estimates of the interdependence in both directions as judged by L or $d_{x,y}$ are obtained for equal values of the coupling strength. This finding is in accordance with expectation and previous findings [15,25] as it reflects the symmetry between the dynamics in this setting. On the other hand, we showed that in nonidentical bidirectionally coupled dynamics equal estimates of interdependence in both directions are obtained for unequal values of the coupling strength. In other words, in the case of nonidentical coupled dynamics, if the coupling strength from the dynamics X to the dynamics Y is stronger than in the opposite direction, this does not always imply that also the interaction from X to Y is higher than for the opposite direction. These findings do not reflect a peculiarity of L or $d_{x,y}$ but are consistent with results of previous studies [15,39], which used state-space [39] and phase-based [15,39] approaches for the characterization of interaction between bidirectionally coupled dynamics. For increasingly different coupled dynamics, equal estimates of the interaction between the dynamics are obtained for increasingly different coupling strength values. Therefore, the coupling strength values do not determine by themselves the real impact that one dynamics exerts on the other.

In order to address this problem we here introduced the notion of the coupling impact. The coupling impact takes into account not only the coupling strength between the dynamics but also the energy of the individual dynamics. As an estimator of this energy we used the variance of the signal that corresponds to the variable through which the dynamics are coupled. We found that equal estimates of interdependence in both directions are obtained for approximately equal coupling impact values, regardless of the asymmetry between the

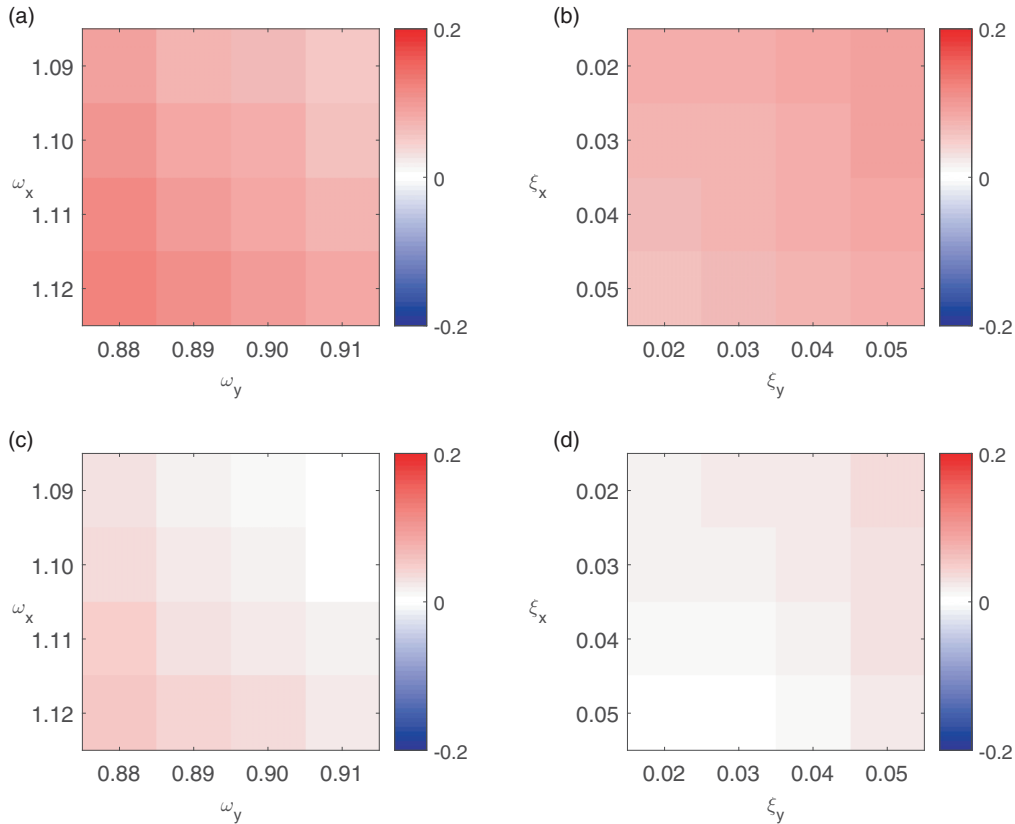


FIG. 5. The coupling impact correctly detects symmetric interactions for the noisy van der Pol oscillators. Values of ρ_ϵ (a, b) and ρ_γ (c, d) for different frequency and noise levels. In the first column we vary the frequencies $\omega_{x,y}$, while the noise levels $\xi_{x,y}$ are fixed to 0.04. On the second one, the frequencies ω_x, ω_y are fixed to 1.1 and 0.9, respectively, and the noise levels $\xi_{x,y}$ vary.

coupled dynamics. Hence, this approach reveals the real impact that one dynamics has on the other much more reliably than the coupling strength.

We choose the variance as a data-driven estimator of the dynamics’ energy because it is a simple and intuitive quantity. Our results show that it is well-suited to address symmetric interactions in nonidentical coupled dynamics. On the other hand, we still at times have a remaining mismatch. In some cases equal estimates of interaction in both directions are obtained for only approximately equal coupling impact values. Hence, an open topic for a future study is to test higher-order moments for the estimation of the dynamics’ energy. Furthermore, we can consider dynamics that are coupled not only diffusively but which have more complex interactions.

It is important to underline the scope of this work. For real-world data one does not know in general the values of the coupling strength of the underlying dynamics. Furthermore, the variance of real-world signals might not reflect well the true energy that one dynamics exerts on the other, but instead depends on the measurement. An important aspect is the path between the place where the dynamics takes place and the location of the measurement device. In electroencephalographic recordings, for example, the activity of the interacting neurons takes place in the brain but electrodes are placed on different positions of the scalp. Moreover, the electrode impedance is not identical across different electrodes. Hence, the variance of electroencephalographic recordings cannot be the real variance of the signal through which the coupling is conveyed. For these

reasons an application of the coupling impact to experimental data is not straightforward.

We also note that noisy dynamics with time-varying parameters can be analyzed with the dynamical Bayesian inference approach [32–35] that reveals the effective connectivity. However, the phase-based approach that we applied here as well as the dynamical Bayesian inference approach are model-based [60], while the state-space approach does not assume any model of the interacting dynamics.

Concluding, we underline that the aim of the present paper is not to propose the coupling impact as a measure to analyze experimental data. Instead, it serves as a way to define symmetric interactions between bidirectionally coupled dynamics, regardless of whether or not they are identical. Therefore, although we follow a data-driven approach our contribution is toward an understanding of dynamical systems.

ACKNOWLEDGMENTS

The authors are grateful to Irene Malvestio for useful discussion and valuable feedback on the manuscript. They acknowledge funding from the Volkswagen foundation and support by the Spanish Ministry of Economy and Competitiveness (Grant No. FIS2014-54177-R). This project has received funding from the European Union’s Horizon 2020 research and innovation programme under the Marie Skłodowska-Curie Grant Agreement No. 642563 (R.G.A.) and CERCA Programme/Generalitat de Catalunya (R.G.A.).

- [1] C. Hiemstra and J. D. Jones, *J. Finance* **49**, 1639 (1994).
- [2] H. Moon and T.-C. Lu, *Sci. Rep.* **5**, 9450 (2015).
- [3] L. Faes, G. Nollo, and A. Porta, *Frontiers Physiol.* **2**, 80 (2011).
- [4] B. Kralemann, M. Frühwirth, A. Pikovsky, M. Rosenblum, T. Kenner, J. Schaefer, and M. Moser, *Nat. Commun.* **4**, 2418 (2013).
- [5] R. G. Andrzejak, K. Lehnertz, F. Mormann, C. Rieke, P. David, and C. E. Elger, *Phys. Rev. E* **64**, 061907 (2001).
- [6] M. D. Fox, A. Z. Snyder, J. L. Vicent, M. Corbetta, D. C. V. Essen, and M. E. Raichle, *Proc. Natl. Acad. Sci. USA* **102**, 9673 (2005).
- [7] I. I. Mikhov and D. A. Smirnov, *Geophys. Res. Lett.* **33**, L03708 (2006).
- [8] M. Paluš, *Phys. Rev. Lett.* **112**, 078702 (2014).
- [9] A. Čenys, G. Lasiene, and K. Pyragas, *Physica D: Nonlin. Phenom.* **52**, 332 (1991).
- [10] S. J. Schiff, P. So, T. Chang, R. E. Burke, and T. Sauer, *Phys. Rev. E* **54**, 6708 (1996).
- [11] J. Arnhold, P. Grassberger, K. Lehnertz, and C. E. Elger, *Physica D* **134**, 419 (1999).
- [12] R. Q. Quiroga, T. Kreuz, and P. Grassberger, *Phys. Rev. E* **66**, 041904 (2002).
- [13] R. G. Andrzejak, A. Kraskov, H. Stögbauer, F. Mormann, and T. Kreuz, *Phys. Rev. E* **68**, 066202 (2003).
- [14] D. Chicharro and R. G. Andrzejak, *Phys. Rev. E* **80**, 026217 (2009).
- [15] M. G. Rosenblum and A. S. Pikovsky, *Phys. Rev. E* **64**, 045202 (2001).
- [16] D. A. Smirnov and B. P. Bezruchko, *Phys. Rev. E* **68**, 046209 (2003).
- [17] B. Schelter, M. Winterhalder, R. Dahlhaus, J. Kurths, and J. Timmer, *Phys. Rev. Lett.* **96**, 208103 (2006).
- [18] B. Kralemann, L. Cimponeriu, M. Rosenblum, A. Pikovsky, and R. Mrowka, *Phys. Rev. E* **76**, 055201 (2007).
- [19] B. Kralemann, L. Cimponeriu, M. Rosenblum, A. Pikovsky, and R. Mrowka, *Phys. Rev. E* **77**, 066205 (2008).
- [20] B. Kralemann, A. Pikovsky, and M. Rosenblum, *Chaos* **21**, 025104 (2011).
- [21] B. Kralemann, A. Pikovsky, and M. Rosenblum, *New J. Phys.* **16**, 085013 (2014).
- [22] T. Schreiber, *Phys. Rev. Lett.* **85**, 461 (2000).
- [23] M. Paluš and A. Stefanovska, *Phys. Rev. E* **67**, 055201 (2003).
- [24] M. Paluš and M. Vejmelka, *Phys. Rev. E* **75**, 056211 (2007).
- [25] I. Vlachos and D. Kugiumtzis, *Phys. Rev. E* **82**, 016207 (2010).
- [26] L. Faes, G. Nollo, and A. Porta, *Phys. Rev. E* **83**, 051112 (2011).
- [27] D. Kugiumtzis, *Phys. Rev. E* **87**, 062918 (2013).
- [28] C. Rummel, M. Müller, G. Baier, F. Amor, and K. Schindler, *J. Neurosci. Methods* **191**, 94 (2010).
- [29] Z. Levnajić, *Eur. Phys. J. B* **86**, 298 (2013).
- [30] Z. Levnajić and A. Pikovsky, *Sci. Rep.* **4**, 5030 (2014).
- [31] V. N. Smelyanskiy, D. G. Luchinsky, A. Stefanovska, and P. V. E. McClintock, *Phys. Rev. Lett.* **94**, 098101 (2005).
- [32] T. Stankovski, A. Duggento, P. V. E. McClintock, and A. Stefanovska, *Phys. Rev. Lett.* **109**, 024101 (2012).
- [33] T. Stankovski, P. V. E. McClintock, and A. Stefanovska, *Phys. Rev. X* **4**, 011026 (2014).
- [34] T. Stankovski, V. Ticcinelli, P. V. E. McClintock, and A. Stefanovska, *New J. Phys.* **17**, 035002 (2015).
- [35] P. T. Clemson and A. Stefanovska, *Phys. Rep.* **542**, 297 (2014).
- [36] A. Attanasio and U. Triacca, *Theor. Appl. Climatol.* **103**, 103 (2011).
- [37] A. Montalto, S. Stramaglia, L. Faes, G. Tessitore, R. Prevete, and D. Marinazzo, *Neural Networks* **71**, 159 (2015).
- [38] R. Q. Quiroga, A. Kraskov, T. Kreuz, and P. Grassberger, *Phys. Rev. E* **65**, 041903 (2002).
- [39] D. A. Smirnov and R. G. Andrzejak, *Phys. Rev. E* **71**, 036207 (2005).
- [40] T. Kreuz, Measuring synchronization in model systems and electroencephalographic time series from epilepsy patients, Ph.D. thesis, University of Wuppertal, 2003.
- [41] T. Kreuz, F. Mormann, R. G. Andrzejak, A. Kraskov, K. Lehnertz, and P. Grassberger, *Physica D: Nonlin. Phenom.* **225**, 29 (2007).
- [42] H. Osterhage, F. Mormann, T. Wagner, and K. Lehnertz, *Phys. Rev. E* **77**, 011914 (2008).
- [43] A. Pikovsky, M. Rosenblum, and J. Kurths, *Synchronization: A Universal Concept in Nonlinear Sciences*, Cambridge nonlinear science series (Cambridge University Press, Cambridge, 2001).
- [44] G. Alba, E. Pereda, S. Mañas, L. D. Méndez, M. R. Duque, A. González, and J. J. González, *Clin. Neurophysiol.* **127**, 1321 (2016).
- [45] P. Papiotis, A computational approach to studying interdependence in string quartet performance, Ph.D. thesis, Universitat Pompeu Fabra, 2015.
- [46] R. G. Andrzejak, D. Chicharro, K. Lehnertz, and F. Mormann, *Phys. Rev. E* **83**, 046203 (2011).
- [47] R. G. Andrzejak, K. Schindler, and C. Rummel, *Phys. Rev. E* **86**, 046206 (2012).
- [48] F. Takens, in *Dynamical Systems and Turbulence, Warwick 1980*, Lecture Notes in Mathematics, Vol. 898, edited by D. Rand and L.-S. Young (Springer, Berlin/Heidelberg, 1981), pp. 366–381.
- [49] J. Theiler, *Phys. Rev. A* **34**, 2427 (1986).
- [50] A Matlab code for the calculation of the measure L can be downloaded from <http://ntsa.upf.edu/downloads/>.
- [51] M. G. Rosenblum, L. Cimponeriu, A. Bezerianos, A. Patzak, and R. Mrowka, *Phys. Rev. E* **65**, 041909 (2002).
- [52] B. Bezruchko, V. Ponomarenko, M. G. Rosenblum, and A. S. Pikovsky, *Chaos* **13**, 179 (2003).
- [53] L. Cimponeriu, M. Rosenblum, T. Fieseler, J. Dammers, M. Schiek, M. Majtanik, P. Morosan, A. Bezerianos, and P. A. Tass, *Prog. Theor. Phys. Suppl.* **150**, 22 (2003).
- [54] R. Mrowka, L. Cimponeriu, A. Patzak, and M. G. Rosenblum, *Am. J. Physiol. Regul. Integr. Comp. Physiol.* **285**, R1395 (2003).
- [55] Note that the directionality index can be also obtained with different ways. A Matlab code for its calculation with all the intermediate steps needed can be downloaded from www.stat.physik.uni-potsdam.de/~mros/damoco2.html.
- [56] C. Tenreiro, *J. Nonparametr. Stat.* **23**, 533 (2011).
- [57] A. S. Pikovsky, M. G. Rosenblum, and J. Kurths, *Europhys. Lett.* **34**, 165 (1996).
- [58] D. García-Álvarez, A. Bahraminasab, A. Stefanovska, and P. V. E. McClintock, *Europhys. Lett.* **88**, 30005 (2009).
- [59] R. P. Brent, *Algorithms for Minimization Without Derivatives* (Prentice-Hall, Englewood Cliffs, 1973).
- [60] M. Rosenblum, L. Cimponeriu, and A. Pikovsky, *Handbook of Time Series Analysis* (Wiley-VCH Verlag, Berlin, 2006), Chap. 7, pp. 159–180.